Systematic weakly nonlinear analysis of interfacial instabilities in Hele-Shaw flows

E. Alvarez-Lacalle, J. Casademunt, and J. Ortín
Departament d'Estructura i Constituents de la Matèria, Universitat de Barcelona, Avinguda Diagonal, 647, E-08028 Barcelona, Spain

(Received 21 November 2000; revised manuscript received 26 January 2001; published 11 June 2001)

We develop a systematic method to derive all orders of mode couplings in a weakly nonlinear approach to the dynamics of the interface between two immiscible viscous fluids in a Hele-Shaw cell. The method is completely general: it applies to arbitrary geometry and driving. Here we apply it to the channel geometry driven by gravity and pressure. The finite radius of convergence of the mode-coupling expansion is found. Calculation up to third-order couplings is done, which is necessary to account for the time-dependent Saffman-Taylor finger solution and the case of zero viscosity contrast. The explicit results provide relevant analytical information about the role that the viscosity contrast and the surface tension play in the dynamics of the system. We finally check the quantitative validity of different orders of approximation and a resummation scheme against a physically relevant, exact time-dependent solution. The agreement between the low-order approximations and the exact solution is excellent within the radius of convergence, and is even reasonably good beyond this radius.

DOI: 10.1103/PhysRevE.64.016302 PACS number(s): 47.20.Ma, 47.20.Hw, 47.54.+r, 47.20.Ky

I. INTRODUCTION

The morphological instability of fluid interfaces in Hele-Shaw flows [1,2] has become a paradigm of interfacial pattern formation in nonequilibrium systems [3–5]. As opposed to the most commonly studied ''bulk'' pattern forming systems [6], the inherent difficulties of free-boundary problems associated with interfacial growth makes the latter even more elusive to analytical treatment. As a prototype of interfacial instabilities in diffusion-limited growth problems (including, for instance, dendritic growth, solidification of mixtures, chemical electrodeposition, flame propagation, etc.) the Saffman-Taylor problem [7] is a relatively simple case, both theoretically and experimentally, well suited for gaining insight into generic dynamical features in the broad context of nonlinear interface phenomena.

The intrinsic difficulty of free-boundary problems is manifest in the fact that the interface dynamics is highly nonlocal. Furthermore, the nature of the instability (except in some cases, such as in directional solidification of binary alloys) usually produces nonsaturated growth, which inevitably results in highly nonlinear dynamics. In bulk instabilities, when the control parameter is near the threshold, the traditional weakly nonlinear techniques lead to a universal description of patterns in terms of amplitude equations based on center manifold reduction [6,8]. These techniques, however, are not so useful for interfacial problems in which nonlinearities do not saturate the growth. This is the case, for instance, of viscous fingering. In the case of the channel geometry (Saffman-Taylor problem) [1,7] the interface restabilizes in a nontrivial morphology (the Saffman-Taylor finger), which keeps growing at a finite rate. For circular geometries [9,10] the patterns do not reach an equivalent steady state and the interplay of tip-splitting events and screening effects may result in a variety of complicated morphologies. In these problems all the weakly nonlinear techniques apply only to a transient in the early nonlinear regime. Nevertheless, compared to the more traditional ones [6,8], the weakly nonlinear analysis developed in this paper is not restricted to situations near the instability threshold, where a separation of scales is exploited. Instead, we expand on the amplitudes of the whole spectrum of modes.

In the traditional Saffman-Taylor problem (channel geometry) the pressure- and gravity-driven instabilities can be formally mapped into each other in the appropriate reference frames, so there is really no different interface dynamics for the two physical situations. The problem, then, contains two independent dimensionless parameters, namely, a dimensionless surface tension B and the viscosity contrast or Atwood ratio A [11]. In the radial geometry, though, there is no such formal mapping. The injection and the centrifugal forcing are not equivalent and three independent parameters must be considered.

The situation most commonly studied in the literature is the high viscosity contrast limit, $A=1$, where one of the two fluids is nonviscous [1] (typically air displacing a viscous fluid). The singular perturbation character of the surface tension B has received most of the attention as being responsible for the subtle mechanism of *steady-state selection*, namely, the fact that surface tension ''selects'' a single-finger solution out of a continuum of solutions for $B=0$ [12–14]. More recently, the crucial role of surface tension in the *dynamics* of fingering patterns has been pointed out. Tanveer and co-workers [15–17] have shown that the exact, nonsingular time-dependent solutions known for the case with $B=0$ may differ significantly from the corresponding solutions with $B\rightarrow 0^+$ after a time, which is of order one (B^0). In practice, this implies that exact solutions of the problem with $B=0$ (including those with no finite time singularities) may lead to completely incorrect asymptotic behavior as compared to the regularized solutions with $B\ll 1$. A careful analysis of these questions may be found in Ref. [18]. Notice, however, that such an analysis is restricted to small B, while in many cases (for instance, for fingers emerging naturally from the linear instability, with the characteristic length scale of the linearly most unstable mode) the effective dimensionless surface tension is necessarily $B\sim 1$. Understanding the dynamics of finger competition in typical experimental conditions thus requires considering relatively large values of B, for which the perturbative techniques of [15–17] fail.

On the other hand, an important role of viscosity contrast A in the dynamics of finger competition has been observed both numerically [11,19] and experimentally [20–22]. A careful characterization of the evolution of the interface has shown that for $A=0$ the finger competition process is ineffective, and that the system does not approach the usual single-finger Saffman-Taylor attractor [23,24]. Although the nature or existence of other attractors is still an open question, it seems that the basin of attraction of the Saffman-Taylor solution does depend on A, and is particularly sensitive to A in the neighborhood of $A\simeq 1$. In any case, it is clear that the viscosity contrast plays also a crucial role in the highly nonlinear regime, and that tuning A in its full range is necessary to elucidate some of the important questions that remain unanswered.

Finally, an interesting interplay between B and A in connection with the selection problem is apparent in that, despite the fact that single-finger stationary solutions of any width do exist for $B=0$ regardless of viscosity contrast A, the only single-finger time-dependent solution of the $A=1$ ($B=0$) problem, which is also a solution for any viscosity contrast A, is the one that fills one half of the channel [25,26], which is precisely the solution selected by surface tension in the limit $B\to 0$. Whether deeper consequences concerning the selection problem can be drawn from this fact is also an open question of considerable interest.

In order to gain analytical insight into these dynamical questions we propose here a systematic weakly nonlinear expansion of the problem of viscous fingering in Hele-Shaw flows, applicable in all traditional setups and the most recent one of rotating flows [27]. The basic reason is to be able to extract information that is nonperturbative in any of the two basic parameters, which are taken as completely arbitrary. The expansion parameter will be basically the mode amplitudes.

In this paper we will focus on unstable stratified flows, for which the approach is necessarily restricted to the early evolution of the interface. Although some of the nontrivial dynamical effects mentioned above are associated with the highly nonlinear regime, it may be useful to know within a controlled approximation to what extent these or other effects already show up in the early stages of nonlinear mode coupling.

For the stable stratified case the weakly nonlinear analysis is obviously valid for long times since all mode amplitudes decay with time. Although this configuration may seem trivial, this is not the case in some situations, for instance, when some external source systematically drives the interface out of its equilibrium state. An example of this is the presence of noise sources, such as the quenched noise associated with a porous medium [28]. In a study of the long-wavelength, low-frequency scaling properties of the interface fluctuations, knowledge of the lowest-order nonlinear terms and their dependence on parameters such as viscosity contrast is crucial. In this context the weakly nonlinear expansion is the starting point of any renormalization group analysis of the relevant terms and of the fixed points of the problem. This line of research is clearly beyond the scope of this paper and will not be pursued here.

The case of centrifugal forcing of Hele-Shaw flows [29] can also be addressed using our formulation. The experimental study of rotating Hele-Shaw flows has revealed a rich variety of new phenomena [27,30,31]. From a theoretical point of view, new classes of exact solutions with $B=0$ have been found [32,33]. The role of rotation in the possible suppression of finite time cusp singularities in the absence of surface tension has been discussed in [34]. From an experimental point of view, important differences in pattern morphology and new dynamical effects have been found for low viscosity contrasts [35]. It thus seems important to have this case included in the weakly nonlinear formalism. The analysis has already been carried out [36] and will be discussed in detail in a separate paper.

The first weakly nonlinear analysis of a viscous fingering problem was carried out by Guo, Hong, and Kurtze [37,38], who studied an intrinsically nonlinear, surface-tension-driven instability. The basic ideas developed here were introduced by Miranda and Widom [39,40] for the standard viscous fingering problem both in channel and circular geometry (with fluid injection). The present work is in part an extension of those previous contributions in several directions, and in part a detailed study of selected particular situations to assess the validity and limitations of the approach.

First of all, we provide a fully systematic methodology that may be carried out to arbitrary order. We apply this technique to derive an equation for the interface evolution in real space up to cubic nonlinearities. When this equation is expressed in Fourier space it reproduces the second- and third-order mode couplings obtained by Miranda and Widom in Ref. [39]. These results are applied to the study of the evolution of the Saffman-Taylor finger of width one-half—a configuration with up-down symmetry where the second order is not present. It is implicit in our approach how further orders can be computed due to the systematics of the method.

In addition, our study extends the earlier results of Miranda and Widom [39,40] with the discussion of the convergence of the weakly nonlinear analysis. We find the explicit exact criterion to ensure uniform convergence of the series. Beyond this condition the series is asymptotic, and different resummation schemes are also explored. The different orders of approximation, including possible resummations, are carefully compared with exact solutions for the case of a single-finger configuration. We find that, in some cases, agreement even at relatively low orders is quite remarkable.

The layout of the rest of the paper is as follows. In Sec. II we introduce the formalism. Section III deals with the derivation of the weakly nonlinear equations and their application to Hele-Shaw flows in channel geometry. Section IV presents a numerical analysis of exact and approximate solutions. The main results and conclusions are summarized in Sec. V.

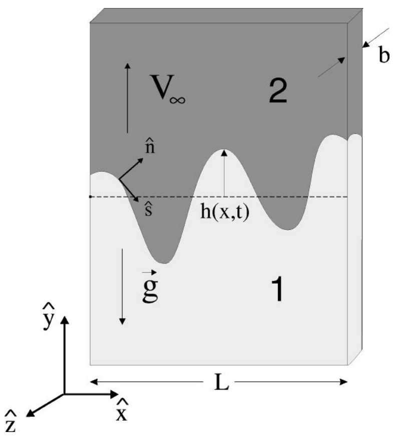

FIG. 1. Sketch of the Hele-Shaw cell in channel geometry.

II. VORTEX SHEET FORMALISM

Let us first consider the Hele-Shaw problem in the channel geometry. We consider fluid 1 (viscosity μ_1, density ρ_1) below fluid 2 (μ_2,ρ_2) (Fig. 1). The $\hat{z}$ axis is perpendicular to the cell. A velocity V_∞ is imposed at infinity in the $\hat{y}$ direction. Gravity points from fluid 2 to fluid 1. The width of the cell is L, the gap between plates is b, and the surface tension between the fluids is σ.

The equations of motion for the interface and the boundary conditions are well known [7]. Here we will use the formulation of Tryggvason and Aref [11]. We introduce the velocity $\vec{U}=(\vec{u}_1+\vec{u}_2)/2$ as the mean of the two limiting values of the velocities from both sides of the interface $(\vec{u}_1,\vec{u}_2)$ at a given point. This velocity $\vec{U}$ can be expressed in terms of the vortex sheet distribution γ at the interface as

$$\vec{U}(s,t)=\frac{1}{2\pi}\mathrm{P}\int\frac{\hat{z}\times[\vec{r}(s,t)-\vec{r}(s',t)]}{|\vec{r}(s,t)-\vec{r}(s',t)|^2}\gamma(s',t)ds', \tag{2.1}$$

where

$$\gamma=2A(\vec{U}\cdot\hat{\mathbf{s}})+2C\hat{\mathbf{y}}\cdot\hat{\mathbf{s}}+2D\kappa_s, \tag{2.2}$$

where s is the arclength, κ is the curvature, and

$$A=\frac{\mu_2-\mu_1}{\mu_2+\mu_1},\quad C=\frac{gb^2(\rho_2-\rho_1)}{12(\mu_2+\mu_1)}+AV_\infty,$$

$$D=\frac{\sigma b^2}{12(\mu_2+\mu_1)},\quad \gamma=(\vec{u}_1-\vec{u}_2)\cdot\hat{s}. \tag{2.3}$$

For the purposes of this work it is convenient to rewrite these equations in terms of the interface height $h(x)$ following [41]. The equations read

$$\vec{U}(x,t)=\frac{1}{2\pi}\mathrm{P}\int_{-\infty}^{+\infty}\frac{(h(x')-h(x),x-x')}{(x-x')^2+[h(x')-h(x)]^2}\tilde{\gamma}(x')dx', \tag{2.4}$$

$$\tilde{\gamma}=2D\kappa_x+2Ch_x+2A\vec{U}\cdot(1,h_x), \tag{2.5}$$

where

$$\tilde{\gamma}=\gamma\sqrt{1+h_x^2},\quad \kappa=\frac{h_{xx}}{(1+h_x^2)^{3/2}}. \tag{2.6}$$

The dependence of h and $\tilde{\gamma}$ on time is not written explicitly.

To complete the definition of the moving boundary problem the continuity of the normal velocity at the interface is required. This means that the velocity in the y direction, dh/dt, projected along the normal direction is equal to the normal component of the average velocity of the interface, $\vec{U}\cdot\hat{n}$,

$$\frac{dh}{dt}=U_{\hat{y}}-U_{\hat{x}}h_x. \tag{2.7}$$

In Sec. III we will consider the interface in the comoving frame ($\overline{h}=0$) and will look for the equation of evolution of $h(x,t)$.

III. SYSTEMATIC WEAKLY NONLINEAR ANALYSIS—CHANNEL GEOMETRY

Our goal in this section is to introduce a systematic method to derive an evolution equation of the interface in real space, to a given order in nonlinear couplings in the channel geometry. The different orders of mode couplings will be ordered as powers of a "book-keeping" parameter ε to be defined below. The evolution of the interface will thus take the form

$$\frac{dh}{dt}=F[h]+\varepsilon G[h]+\varepsilon^2 I[h]+\cdots, \tag{3.1}$$

where $F[h],G[h]$, etc. are nonlocal operators on the function $h(x,t)$, including nonlinearities of order $n+1$ in the term of order ε^n. The small parameter ε is defined as the ratio of two lengths, $\varepsilon=w/L$. We take w as a measure of the characteristic scale of variation of the interface $h(x)$, while L is either the width of the cell or, alternatively, the characteristic scale of variation in the x direction. The weakly nonlinear regime is defined by the condition $w\ll L$.

The order ε^0 in Eq. (3.1) corresponds to the linearized equation. The order ε^1, when written in Fourier space, corresponds to the result of Miranda and Widom [39]. Here we will perform the explicit calculation to one order higher in ε (up to $I[h]$), which is the leading nonlinear contribution in several important cases, such as those discussed in Sec. III D.

A. Dimensionless equations, expansion and convergence

We scale the interface height with w, the coordinate x with L, and the time with L/C, where the velocity C has been defined in Eq. (2.3).

The Eqs. (2.4), (2.5), (2.6), and (2.7) become

$$\vec{U}(x,t)$$

$$=\frac{1}{2\pi}\mathrm{P}\int_{-\infty}^{+\infty}\frac{(\varepsilon[h(x')-h(x)],x-x')}{(x-x')^2\left\{1+\varepsilon^2\left[\frac{h(x')-h(x)}{x'-x}\right]^2\right\}}\tilde{\gamma}(x')dx', \tag{3.2}$$

$$\tilde{\gamma}=2B\kappa_x+2\varepsilon h_x+2A\vec{U}\cdot(1,\varepsilon h_x), \tag{3.3}$$

where

$$B=\frac{\sigma b^2}{12CL^2(\mu_1+\mu_2)}, \quad \kappa=\frac{\varepsilon h_{xx}}{(1+\varepsilon^2 h_x^2)^{3/2}}, \tag{3.4}$$

and

$$\frac{dh}{dt}=\frac{1}{\varepsilon}U_{\hat{y}}-U_{\hat{x}}h_x. \tag{3.5}$$

The starting point of our approach is an expansion of $\vec{U}$, $\tilde{\gamma}$, and κ in powers of ε. Notice that the term $[h(x')-h(x)]^2/[x'-x]^2$ between curly brackets in Eq. (3.2) is bounded provided that h_x does not diverge. Equation (3.5) thus takes the form

$$\frac{dh}{dt}=\frac{1}{\varepsilon}U_{\hat{y}}^{(0)}+U_{\hat{y}}^{(1)}-h_xU_{\hat{x}}^{(0)}+\varepsilon(U_{\hat{y}}^{(2)}-h_xU_{\hat{x}}^{(1)})+\cdots. \tag{3.6}$$

Before pursuing the calculation in detail, let us point out that the ε expansion in Eq. (3.6) has a finite radius of convergence. This is guaranteed by the properties of uniform convergence of both the expansion of the inverse of the denominator in Eq. (3.2) and the curvature. These properties allow us to commute the expansion with the integral in Eq. (3.2) and yield a convergent series of the form (3.6). The radius of convergence of the expansion in Eq. (3.2) is given by the condition $\varepsilon^2[h(x')-h(x)]^2/[x'-x]^2<1$, while the convergence of the curvature expansion is ensured by the condition $\varepsilon^2h_x^2<1$. By virtue of the mean value theorem, a necessary and sufficient condition for $\varepsilon^2[h(x')-h(x)]^2/[x'-x]^2<1$ for any two values x,x' is that $\varepsilon^2h_x^2<1$ for all x. Therefore, the two conditions are equivalent. In the original nonscaled variables, this condition for convergence reads $\mathrm{Max}(|h_x|)<1$. In conclusion, if $|h_x|<1$ in the whole domain of integration, then the ε expansion converges. If the condition is not fulfilled in some intervals, then Eq. (3.6) is an asymptotic expansion. Even in this case, the expansion contains useful information about the original problem.

An interesting case is $A=0$ that makes the vorticity independent of $\vec{U}$ in Eq. (3.2) so that Eq. (3.5) becomes a closed equation for $h(x,t)$. Then, in Eq. (3.6) it is easy to show that $U_{\hat{y}}^{(n)}=0$ when n is even and $U_{\hat{x}}^{(n)}=0$ when n is odd, a property that makes the even power terms of the expansion in Eq. (3.6) vanish.

B. First- and second-order expansion (ε^0 and ε^1)

Following the scheme introduced in the previous section, Eq. (3.2) produces

$$U_{\hat{x}}^{(0)}=0,\quad U_{\hat{x}}^{(1)}=\frac{1}{2\pi}\mathrm{P}\int_{-\infty}^{+\infty}\frac{h(x')-h(x)}{(x-x')^2}\tilde{\gamma}^{(0)}(x')dx', \tag{3.7}$$

$$U_{\hat{y}}^{(0)}=\frac{1}{2\pi}\mathrm{P}\int_{-\infty}^{+\infty}\frac{\tilde{\gamma}^{(0)}(x')}{x-x'}dx',$$

$$U_{\hat{y}}^{(1)}=\frac{1}{2\pi}\mathrm{P}\int_{-\infty}^{+\infty}\frac{\tilde{\gamma}^{(1)}(x')}{x-x'}dx'. \tag{3.8}$$

Since $\tilde{\gamma}^{(0)}=2B\kappa_x^{(0)}+2AU_{\hat{x}}^{(0)}=0$ we get $U_{\hat{x}}^{(1)}=U_{\hat{y}}^{(0)}=0$. With this result we can study the first-order term in the vorticity equation,

$$\tilde{\gamma}^{(1)}(x)=2B\kappa_x^{(1)}+2h_x+2AU_{\hat{x}}^{(1)}+2Ah_xU_{\hat{y}}^{(0)}. \tag{3.9}$$

Taking into account the definition of the Hilbert transform,

$$H[f(x')]=\frac{1}{\pi}\mathrm{P}\int_{-\infty}^{+\infty}\frac{f(x')}{x'-x}dx'. \tag{3.10}$$

Equation (3.6) up to order ε^0 reads

$$\frac{dh}{dt}=-H[Bh_{x'x'x'}+h_{x'}]. \tag{3.11}$$

The linear operator $F[h]$ in Eq. (3.1) thus reads explicitly

$$F[h]=\frac{1}{\pi}\mathrm{P}\int_{-\infty}^{+\infty}\frac{(h+Bh_{x'x'})_{x'}}{x-x'}dx'. \tag{3.12}$$

Writing $h(x,t)$ as a superposition of Fourier modes in Eq. (3.11) we recover the linear dispersion relation

$$\frac{\dot{\delta}_k(t)}{\delta_k(t)}=\lambda(k)=|k|(1-Bk^2). \tag{3.13}$$

We will take k as an integer but we should bear in mind that, upon restoring dimensions, k should become $(2\pi/L)n$, where n is an integer.

Let us pursue the systematics of the method by computing the next order in ε in Eq. (3.5),

$$\frac{dh}{dt}=U_{\hat{y}}^{(1)}+\varepsilon U_{\hat{y}}^{(2)}=F[h]+\varepsilon G[h]. \tag{3.14}$$

The computation of $U_{\hat{y}}^{(2)}$ requires an expression of the vorticity up to second order. This includes the evaluation of $U_{\hat{x}}^{(2)}$, which must be computed from the first-order term of the vorticity. We get

$$U_{\hat{x}}^{(2)}=H[(h(x')f(x'))_{x'}]-h(x)H[f_{x'}(x')], \tag{3.15}$$

with $f(x)\equiv(Bh_{xx}+h)_x=\tilde{\gamma}^{(1)}(x)/2$, and

$$U_{\hat{y}}^{(2)}=A\{H[h_{x'}H[f(x'')]]+H[h(x')H[f_{x''}(x'')]]+(hf)_x\}. \tag{3.16}$$

Taking the Fourier transform, we obtain

$$\dot{\delta}_k=\lambda(k)\delta_k+\varepsilon A|k|\sum_{s=-\infty}^{+\infty}[1-\mathrm{sgn}(ks)]\lambda(s)\delta_s(t)\delta_{k-s}(t), \tag{3.17}$$

which coincides with the result of Miranda and Widom in Ref. [39].

C. Third-order expansion (ε^2)

The expansion to order ε^2 is necessary to account for the lowest-order nonlinearities in the case of zero viscosity contrast, and for other relevant situations such as the time-dependent Saffman-Taylor finger solutions (Sec. III D). We now have

$$\frac{dh}{dt}=O(\varepsilon^0)+O(\varepsilon^1)+\varepsilon^2(U_{\hat{y}}^{(3)}-h_xU_{\hat{x}}^{(2)})+\cdots. \tag{3.18}$$

We have already computed $U_{\hat{x}}^{(2)}$ in Eq. (3.15). On the other hand

$$U_{\hat{y}}^{(3)}=-\frac{1}{2}H[\tilde{\gamma}^{(3)}(x')]+\frac{1}{2\pi}\mathrm{P}\int_{-\infty}^{+\infty}\frac{[h(x')-h(x)]^2}{(x'-x)^3}\tilde{\gamma}^{(1)}(x')dx'. \tag{3.19}$$

Integrating twice by parts, the last integral can also be written as a Hilbert transform. After some algebra we obtain the explicit form of the operator $I[h]$ containing the cubic nonlinearities in Eq. (3.1), which reads

$$I[h]=\frac{3}{2}H[g(x')]+\frac{1}{2}H[(f(x')[h(x)-h(x')]^2)_{x'x'}]-h_xH[(f(x')[h(x')-h(x)])_{x'}]+V[h,A] \tag{3.20}$$

with

$$V[h,A]=A^2H[h(x')H[\tau_{x''}(x'')]+h_{x'}(x')H[\tau(x'')]]+A^2(h\tau)_x, \tag{3.21}$$

and

$$g(x)=B(h_{xx}h_x^2)_x,\quad \tau(x)=U_{\hat{x}}^{(2)}+h_xU_{\hat{y}}^{(1)}=\frac{\tilde{\gamma}^{(2)}(x)}{2A}. \tag{3.22}$$

The same result in Fourier space takes the form

$$\dot{\delta}_k(t)=O(1,\varepsilon)+\varepsilon^2\sum_{s,l=-\infty}^{+\infty}\delta_l\delta_{s-l}\delta_{k-s}\left[A^2T(k,s,l)-\frac{3}{2}BY(k,s,l)+W(k,s,l)\right], \tag{3.23}$$

with

$$T(k,s,l)=|k||s|\lambda(l)[1-\mathrm{sgn}(ks)][1-\mathrm{sgn}(ls)], \tag{3.24}$$

$$Y(k,s,l)=|k|l^2(s-l)(k-s), \tag{3.25}$$

$$W(k,s,l)=\left[l\left(\frac{l}{2}+k-s\right)-sk\,\mathrm{sgn}(ls)+\frac{k^2}{2}\mathrm{sgn}(kl)\right]\lambda(l). \tag{3.26}$$

This result can be shown to be equivalent to that of Ref. [39].

It is clear that the viscosity contrast in Eq. (3.23) is squared because of the reflection symmetry (the simultaneous change $A\to-A$ and $h\to-h$ is a dynamical symmetry of the problem). Symmetry reasons alone, however, do not allow us to discard a three-mode-coupling contribution when $A=0$. We see from our calculation that three-mode coupling is indeed present independently of A.

Following this scheme, the fourth order will carry a contribution proportional to A, and another proportional to A^3, for symmetry reasons. The fifth order will carry a contribution independent of A and two others, proportional to A^2 and A^4, respectively. This scheme will continue for subsequent orders. For further details on the reflection symmetry see [39].

D. Analysis of the time-dependent single-finger solution

In this section we perform a detailed analysis of the weakly nonlinear expansion in cases where exact solutions are known, namely, single-finger configurations with $B=0$. This enables the study of how exact properties of solutions show up at the different orders, particularly concerning the role of viscosity contrast A.

At this point it is worth recalling that the case $A=1$ allows for a continuum of Saffman-Taylor finger solutions corresponding to different finger widths. A continuum of time-dependent exact solutions, leading to those stationary states, is also known for $A=1$. However, for $A\neq1$ only that of width $\lambda=\frac{1}{2}$ remains a solution, where λ is the ratio of the finger width to the width of the channel. This result, which has been recently addressed in Ref. [26] although it was first discovered in Ref. [25], shows an intriguing connection between the width selection problem and the dynamical role of viscosity contrast. Here we will analyze the interplay between A and λ in the early nonlinear regime and elucidate at what stage of the nonlinear dynamics does the viscosity contrast $A\neq1$ prevent the possibility of having $\lambda\neq\frac{1}{2}$.

From now on we consider $L=2\pi,\quad B=0,\quad C=1$, and we take $(1-\lambda)C=(1-\lambda)\equiv\eta/2$ as scaling velocity . Conformal mapping techniques enable us to write the single-finger solution of this problem in the form [25,26]

$$f(w,t)=-\ln w+d(t)+\eta\ln[1-\alpha(t)w], \tag{3.27}$$

where $f(w,t)=y+ix$ is an analytic function inside the unit disk in the w complex plane, which maps this disk onto the physical region occupied by the more viscous fluid. The interface is obtained in a parametric form by setting $w=e^{i\theta}$. The functions $\alpha(t)$, $d(t)$ verify

$$\dot{d}(t)=\frac{\eta}{2-\eta}\left[\frac{\eta}{2}-\frac{\dot{\alpha}(t)}{\alpha(t)}\right], \tag{3.28}$$

$$\frac{\dot{\alpha}(t)}{\alpha(t)}=\frac{\eta}{2+\eta(\eta-2)+\eta(2-\eta)\dfrac{1+\alpha^2(t)}{1-\alpha^2(t)}}. \tag{3.29}$$

To obtain an expression for $h(x)$ in the weakly nonlinear regime of the evolution, $\alpha(t)$ and $d(t)$ are expanded in powers of a small parameter ν,

$$d(t)=d^{(0)}(t)+\nu d^{(1)}(t)+\nu^2 d^{(2)}(t)+\cdots,\quad \alpha(t)=\nu\alpha^{(0)}(t)+\nu^2\alpha^{(1)}(t). \tag{3.30}$$

Introducing these expansions in Eqs. (3.28) and (3.29) we obtain

$$\dot{d}^{(0)}=\dot{d}^{(1)}=0,\quad \dot{d}^{(2)}=\frac{\eta^3}{2}(\alpha^{(0)})^2(t),$$

$$\dot{d}^{(3)}=\eta^3\alpha^{(0)}\alpha^{(1)},\ \ldots, \tag{3.31}$$

$$\dot{\alpha}^{(0)}=\frac{\eta}{2}\alpha^{(0)},\quad \dot{\alpha}^{(1)}=\frac{\eta}{2}\alpha^{(1)},$$

$$\dot{\alpha}^{(2)}=\frac{\eta}{2}[\alpha^{(2)}-\eta(2-\eta)(\alpha^{(0)})^3],\ \ldots, \tag{3.32}$$

which will be useful later. From Eqs. (3.27) and (3.28) we obtain

$$\begin{aligned} y=h={}&-\nu\eta\alpha^{(0)}\cos\theta-\nu^2\left[\eta\alpha^{(1)}\cos\theta+\frac{\eta}{2}(\alpha^{(0)})^2\right.\\ &\left.\times\cos2\theta-d^{(2)}\right]-\nu^3\left[\eta\alpha^{(2)}\cos\theta+\eta\alpha^{(0)}\alpha^{(1)}\cos2\theta\right.\\ &\left.+\frac{\eta}{3}(\alpha^{(0)})^3\cos3\theta-d^{(3)}\right]+O(\nu^4), \end{aligned} \tag{3.33}$$

$$x=-\theta-\nu\eta\alpha^{(0)}\sin\theta-\nu^2\left[\eta\alpha^{(1)}\sin\theta+\frac{\eta}{2}(\alpha^{(0)})^2\sin2\theta\right]+O(\nu^3). \tag{3.34}$$

This last equation can be inverted in a systematic way to get

$$\theta=-x+\nu\eta\alpha^{(0)}\sin x+\nu^2\left[\eta\alpha^{(1)}\sin x+\frac{\eta}{2}(1-\eta)\times(\alpha^{(0)})^2\sin2x\right]+O(\nu^3). \tag{3.35}$$

Expanding the cosine functions in Eq. (3.33) we obtain the following expression for $h(x,t)$:

$$\begin{aligned} h(x,t)={}&-\nu\eta\alpha^{(0)}\cos x-\nu^2\eta\left[\alpha^{(1)}\cos x\right.\\ &\left.+\frac{1-\eta}{2}(\alpha^{(0)})^2\cos2x\right]\\ &+\nu^3\eta\left\{(\eta-1)\alpha^{(0)}\alpha^{(1)}\cos2x\right.\\ &+\left[\frac{3\eta}{8}(\eta-2)(\alpha^{(0)})^3-\alpha^{(2)}\right]\cos x\\ &\left.+\left[\frac{3\eta}{8}(2-\eta)-\frac{1}{3}\right](\alpha^{(0)})^3\cos3x\right\}+O(\nu^4). \end{aligned} \tag{3.36}$$

In order to follow the scheme developed in the previous section, we must measure $h(x,t)$ in units of its characteristic amplitude ν. In this way, the previous equation (3.36) takes the form

$$h=h^{(0)}+\nu h^{(1)}+\nu^2h^{(2)}+O(\nu^3), \tag{3.37}$$

where $h(x,t)$ now represents $h(x,t)/\nu$, and the small parameter ν is directly comparable to the small parameter ε of the previous section. The expression for $h(x,t)$ can be regarded as a series of modes of decreasing amplitude in our expansion (3.1) (written in the units of this problem), and matching the corresponding powers in either ε or ν we obtain

$$\frac{dh^{(0)}}{dt}=\frac{\eta}{2}F[h^{(0)}] \tag{3.38}$$

to order ε^0.

This identity can be verified (independently of A) by substituting the expression for $h^{(0)}$ and using Eqs. (3.32) and (3.11) for the left- and right-hand side, respectively. At order ε we have

$$\frac{dh^{(1)}}{dt}=\frac{\eta}{2}(F[h^{(1)}]+G[h^{(0)},h^{(0)}]). \tag{3.39}$$

The second term of the right-hand side gives no contribution and we obtain an interesting result: the equation at order ε is verified independently of η and A. Hence, we cannot establish the difference between $A=1$ (compatible with any η) and $A\neq1$ (compatible only with $\eta=1$) to this order.

The difference between these two situations arises at order ε^2,

$$\frac{dh^{(2)}}{dt}=\frac{\eta}{2}(F[h^{(2)}]+G[h^{(0)},h^{(1)}]+L[h^{(0)},h^{(0)},h^{(0)}]). \tag{3.40}$$

Since the left-hand side of the equation involves only the modes $\cos x$, $\cos 2x$, and $\cos 3x$, the right-hand side of the equation must include these same modes with the same coefficients. The coefficients for $\cos 2x$ and $\cos 3x$ are easily matched. For $\cos x$ the left-hand side reads

$$\left[\frac{\eta^3(\eta-2)}{16}(\alpha^{(0)})^3-\frac{\eta^2}{2}\alpha^{(2)}\right]\cos x, \tag{3.41}$$

where we have used Eq. (3.32), and the right-hand side reads

$$\left[\frac{3\eta^3(\eta-2)}{16}(\alpha^{(0)})^3-\frac{\eta^2}{2}\alpha^{(2)}\right]\cos x +A\frac{\eta^3(1-\eta)}{4}(\alpha^{(0)})^3\cos x+\frac{\eta^4}{8}(\alpha^{(0)})^3\cos x. \tag{3.42}$$

Hence, the requirement for matching the coefficients on both sides is

$$\frac{\eta^3}{4}(1-\eta)=A\frac{\eta^3}{4}(1-\eta), \tag{3.43}$$

which is always true if $\eta=1$ ($\lambda=\frac{1}{2}$), but for $\eta\neq 1$ ($\lambda\neq\frac{1}{2}$) it requires $A=1$. This result shows that the nontrivial relationship between A and λ, which is known from exact solutions, is already manifest at the early nonlinear stages of the dynamics. This clearly illustrates the potential usefulness of the weakly nonlinear expansion at a purely analytical level, in that a dynamical property of the problem that must be satisfied at all orders (in this case the incompatibility of $A\neq 1$ and $\lambda\neq\frac{1}{2}$) may be detected at a low order in the expansion without having to know the exact solution to all orders.

If we pursue the expansion to higher orders, the general expression for $h^{(n)}$ takes the form

$$h^{(n)}=\sum_{k=1}^{n+1}\beta_k^{(n)}(t)\cos(kx), \tag{3.44}$$

where each coefficient is a function of $\alpha(t)$. The even modes of the solution with $\eta=1$ have zero coefficients because they must remain invariant under a change of sign and translation by π.

So far in this section we have restricted ourselves to $B=0$ for comparison with exact results. However, we can also carry out the analysis for $B\neq 0$. It can be shown that the structure of the expression (3.44) is preserved in this case. The coefficients $\beta_k^{(n)}(t)$ are obtained as solutions of a set of differential equations that contain the surface tension B. For instance, to third order we have

$$h(x,t)=(\beta_1^{(0)}+\varepsilon\beta_1^{(1)}+\varepsilon^2\beta_1^{(2)})\cos x+(\varepsilon\beta_2^{(1)}+\varepsilon^2\beta_2^{(2)})\cos 2x+\varepsilon^2\beta_3^{(2)}\cos 3x, \tag{3.45}$$

which, introduced in Eq. (3.1), leads to the following equations:

$$\dot\beta_1^{(0)}=V_0(1-B)\beta_1^{(0)},\quad \dot\beta_1^{(1)}=V_0(1-B)\beta_1^{(1)},$$
$$\dot\beta_2^{(1)}=2V_0(1-4B)\beta_2^{(1)},\quad \dot\beta_2^{(2)}=2V_0(1-4B)\beta_2^{(2)},$$
$$\dot\beta_3^{(2)}=3V_0(1-9B)\beta_3^{(2)}-\frac{9BV_0}{8}(\beta_1^{(0)})^3,$$
$$\dot\beta_1^{(2)}=V_0(1-B)\beta_1^{(2)}+AV_0(1-B)\beta_2^{(1)}\beta_1^{(0)}-\frac{V_0}{8}(2-5B)(\beta_1^{(0)})^3, \tag{3.46}$$

once the dimensions are reintroduced. In this way we can also see how surface tension perturbs the dynamics in the weakly nonlinear regime. Clearly, at these early stages of the nonlinear evolution there is no sign of the singular perturbation character of surface tension, which, during the later stages of the evolution, will be responsible for the selection of the steady state [1].

IV. NUMERICAL STUDY OF AN EXACT SOLUTION AND ITS WEAKLY NONLINEAR APPROXIMATION

The purpose of this section is to put the weakly nonlinear analysis to the test, as a quantitative approximation. We will check it against an exact time dependent solution of the case $B=0$ that evolves towards the Saffman-Taylor finger of width $\lambda=\frac{1}{2}$ in the channel geometry. This will allow us to check how fast the convergence of the expansion is and how accurate it may be even beyond its radius of convergence, when it becomes an asymptotic series.

We define F as the ratio between the maximum height of the interface (at the finger tip) and half the width of the cell (in our case $L=2\pi$). F is a dimensionless amplitude, which is proportional to ε and thus measures how deep the system is within the nonlinear regime. Furthermore, since the system is described by the evolution of a curve, it may also be convenient to have a more global characterization of its configuration in order to compare the exact result and the different approximations. We propose the use of the flux Φ, defined as the total amount of fluid 1 per unit length and unit time flowing across the horizontal line located at the mean interface position [18].

A. The time-dependent exact solution with $B=0$ and $\lambda=\frac{1}{2}$

An explicit solution of the problem without surface tension ($B=0$) and valid for any viscosity contrast A, describing the growth of a single finger that asymptotically fills half of the channel ($\lambda=\frac{1}{2}$), can be obtained from Eqs. (3.27), (3.28), and (3.29). This reads

$$f(w,t)=-\ln w+V_ot+a(0)+\ln[\sqrt{1+\{b(0)^2-1\}\exp(2V_ot)}+w], \tag{4.1}$$

with $a(0)$ and $b(0)$ as initial constants and $b(0)\geqslant 1$. Since this solution is valid for any A, particularly $A=0$, all terms

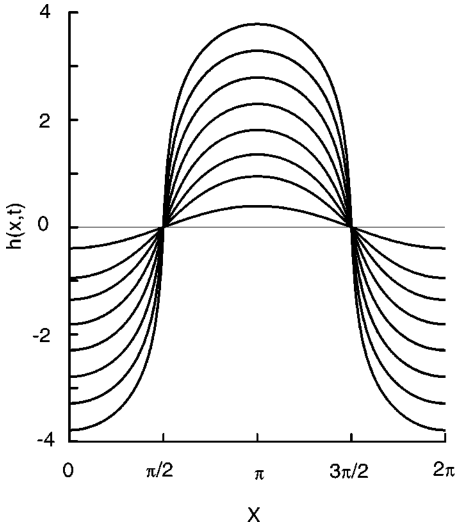

FIG. 2. Evolution of the interface at different values of πF.

of the weakly nonlinear equation (3.1) depending on A will necessarily have no contribution.

We will take the following values for the parameters:

$$V_o=\frac{1}{2},\quad b(0)=\frac{1}{\nu}=1000,\quad a(0)=\ln\nu+\frac{\nu^2}{2}. \tag{4.2}$$

Figure 2 shows the evolution of the interface for this solution. When $F\simeq1$ the finger shape is indistinguishable from the stationary Saffman-Taylor solution (Fig. 3), except near the points $x=\pi/2$ and $x=3\pi/2$ when the asymptotes of the finger must develop at infinite time. When $F=1/\pi$, the slope of the interface becomes 1 at these two points and the series (3.1) loses its convergence, according to the discussion of Sec. III A.

In Fig. 4 we present the amplitude of the Fourier modes of the exact solution. It is clear that relatively few modes suffice to accurately reproduce the stationary finger shape in the tip region.

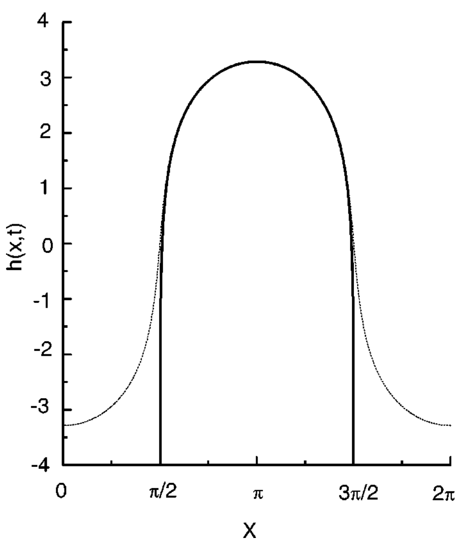

FIG. 3. Comparison of the exact solution [Eq. (4.1)] at $F=1$ (thin line) and the Saffman-Taylor stationary finger (thick line).

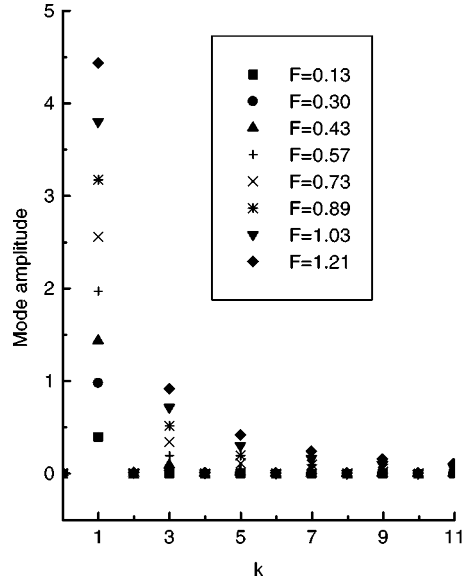

FIG. 4. Amplitude of the Fourier modes of the exact solution at consecutive values of F.

B. Expansion of the exact solution

In Sec. III D we expanded the exact solution (3.27) in a small parameter ν. This expansion revealed a hierarchy of amplitudes of the different modes for an initial condition close to the planar interface. The solution (4.1) can be expanded similarly and yields

$$\nu=\frac{1}{b(0)},\quad \alpha(t)=-\frac{\nu}{b(t)},\quad d(t)=V_o t+\ln b(t),$$

$$b(t)=\sqrt{\nu^2+(1-\nu^2)\exp(2V_o t)}. \tag{4.3}$$

In agreement with Eq. (3.36), and using the same parameters as in the previous section, we obtain up to third order,

$$h(x,t)=\nu e^{t/2}\cos x+\nu^3\left[\left(\frac{1}{2}e^{t/2}-\frac{1}{8}e^{3t/2}\right)\cos x - \frac{1}{24}e^{3t/2}\cos 3x\right]. \tag{4.4}$$

The exact flux Φ can be easily computed from the stream function, which in turn can be related to the form of the mapping equation (4.1) (see, for instance, Ref. [18]). In Figs. 5 and 6 we compare the flux Φ of the approximate result above with the exact result coming from Eq. (4.1). We clearly observe that the first correction to the linear regime improves the flux (to a 5% accuracy) from $F\simeq0.12$ to $F\simeq0.17$. The amplitude of the mode $k=1$ (Fig. 7) is fairly well reproduced by the linear approximation up to $F\simeq0.20$, and the correction of order ν^3 gives a value for the mode $k=3$ that is reasonably good up to $F\simeq0.20$ (Fig. 8) and improves the mode $k=1$ almost until $F\simeq0.25$. Above these values of F the deviation from the exact interface is exponential.

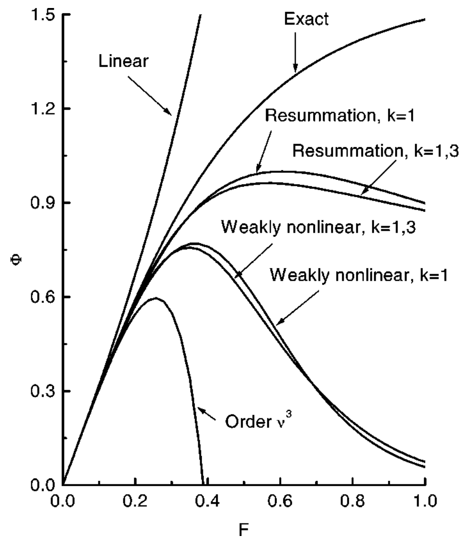

FIG. 5. Flux Φ as a function of the factor F for different approximations (see text for details).

Notice that the expansion up to ν^3 considered here does not account for the complete three-mode coupling of Eq. (3.23) that contains part of the higher orders in ν. This explains why going from order ν (linear) to order ν^3 only slightly improves the shape of the finger, the flux Φ, and the amplitude of the mode $k=1$.

C. Weakly nonlinear expansion

In this section we study the mode-coupling equation (3.23). We solve this equation in cases where only modes $k=1$ and $k=1,3$ are present, and compare the result with both the exact solution and the approximation to order ν^3 introduced in the two previous sections.

We consider the initial condition $\beta_1(0)=\varepsilon=0.001$ for the first mode and zero for the rest of the modes. We use Eq.

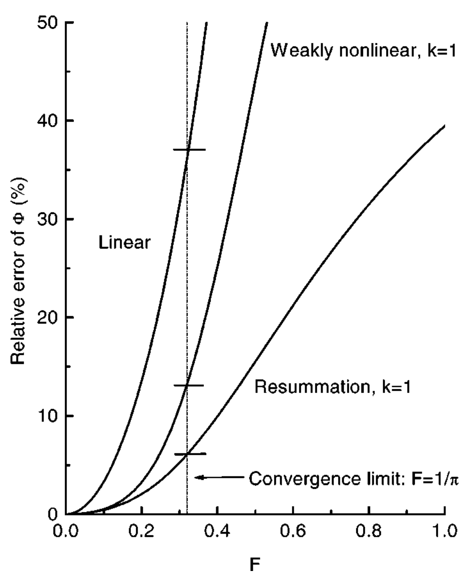

FIG. 6. Relative error of the flux Φ as a function of the factor F for different approximations (see text for details).

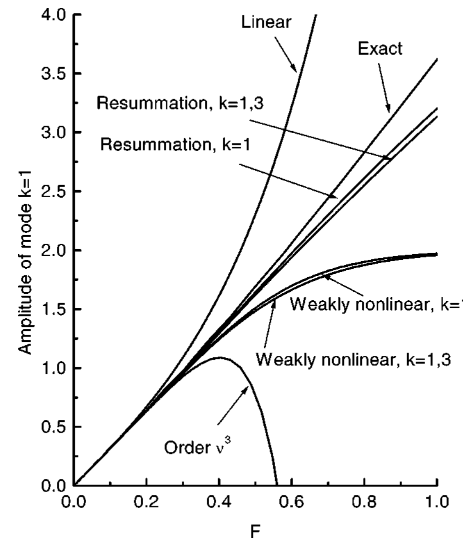

FIG. 7. The first-mode amplitude as a function of the factor F for different approximations (see text for details).

(3.23) recalling that, since β_i represent the amplitudes of the cosine functions, $\delta_i=\beta_i/2$. The result is that the modes $k \neq 1$ remain zero and Eq. (3.23) reduces to

$$\dot{\beta}_1=\frac{1}{2}\beta_1-\frac{1}{8}\beta_1^3, \tag{4.5}$$

which can be solved analytically and yields

$$\beta_1(t)=\frac{\varepsilon\exp(0.5t)}{\sqrt{1+0.25\varepsilon^2[\exp(t)-1]}}, \tag{4.6}$$

where we see that the mode $k=1$ saturates to a finite value as $t\to\infty$. Returning to Figs. 5 and 6, we see that the flux Φ approximates the exact value to within 5% until $F\simeq 0.23$.

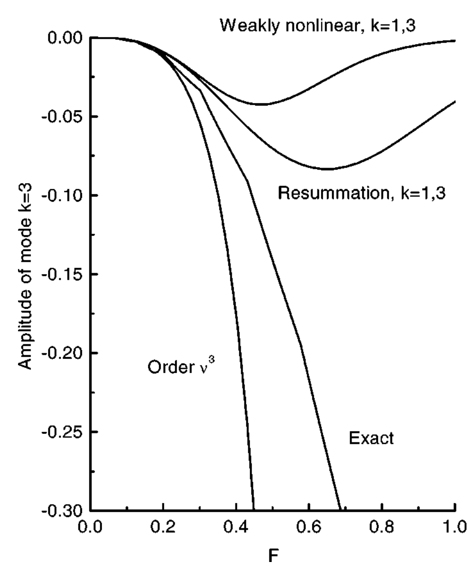

FIG. 8. The third-mode amplitude as a function of the factor F for different approximations (see text for details).

Figure 7 shows that the amplitude of the first mode starts deviating significantly from the exact solution around $F \simeq 0.40$.

Next, we add the third mode to Eq. (3.23) with the initial condition $\beta_1 = \varepsilon + 3\varepsilon^3/8$ and $\beta_3 = \varepsilon^3/24$. The set of equations to be solved numerically is

$$\dot{\beta}_1 = \frac{1}{2}\beta_1 - \frac{1}{8}\beta_1^3 - \frac{5}{4}\beta_3^2\beta_1 + \frac{1}{4}\beta_1^2\beta_3, \tag{4.7}$$

$$\dot{\beta}_3 = \frac{3}{2}\beta_3 - \frac{3}{4}\beta_1^2\beta_3 - \frac{27}{8}\beta_3^3. \tag{4.8}$$

As shown in Figs. 5 and 8 the flux does not improve significantly, while the amplitude of the mode $k=3$ remains acceptable almost until $F \simeq 0.25$, and improves the previous result by more than 50% almost until $F \simeq 0.33$. Beyond this value of F the third mode falls to zero due to the second term on the right-hand side of Eq. (4.8), proportional to $\beta_1^2\beta_3$ but negative. This is a sign that higher-order terms, such as order $\beta_1^4\beta_3$, become important when β_1 is of order one.

From this study we can conclude that using only two modes and the lowest-order nonlinear correction for this case (involving three-mode couplings), both the shape of the interface and the total flux are reasonably well described within the whole range of convergence of the series (up to $F \simeq 1/\pi$). This indicates that the weakly nonlinear description of the problem works remarkably well at the quantitative level, at least in some physically relevant cases. To what extent this conclusion holds for more complicated situations, for instance, those involving competition of different fingers, remains an open question.

D. Partial resummation

According to Eq. (3.23), we can write a closed equation for the mode $k=1$, which is correct up to third-order couplings, in the form

$$\dot{\beta}_1 = \frac{1}{2}\beta_1 - \frac{1}{4}\beta_1^2\dot{\beta}_1, \tag{4.9}$$

where the mode $k=3$ has been initially set to zero.

This equation follows from Eq. (4.5) using the fact that $\frac{1}{2}\beta_1 = \dot{\beta}_1$ to first order.

The presence of $\dot{\beta}_1$ on the right-hand side gives rise to terms of order higher than β_1^3. Thus, solving this equation amounts to doing a partial resummation of these higher-order terms. This kind of closed differential equation was already obtained in Ref. [39]. In our approach this differential equation is obtained in a systematic way by identifying the terms $\lambda(n)\beta_n$ and replacing them with $\dot{\beta}_n$. For example, in Eq. (3.23) the term $T(k,s,l)$ could have been partially resummated in the two-mode coupling differential equation.

The solution of Eq. (4.9) yields the transcendental form

$$t = 2\ln\left(\frac{\beta_1}{\varepsilon}\right) + \frac{1}{4}(\beta_1^2 - \varepsilon^2). \tag{4.10}$$

A numerical computation of the flux based on this equation shows a dramatic improvement up to $F \simeq 1/\pi$ (See Fig. 5 where it is labeled as ''Resummation, $k=1$,'' as in the other figures). It is surprising and remarkable that the equation for a single mode, including the resummation suggested by the first nonlinear correction, reproduces the exact solution to a great accuracy in the full range of convergence and defines an excellent approximation further inside the nonlinear regime. This suggests that this kind of resummation is not arbitrary and might have a deeper physical justification.

In addition, we obtain an amplitude for the mode $k=1$ within 10% accuracy up to $F \simeq 0.8$, and it is still quite accurate until $F=1$. Although the exact spectrum shows the increasing importance of the mode $k=3$ at these values of F, the agreement between the exact result and this approximation for a single mode $k=1$ is quite remarkable.

We recall that the series converges up to $F \simeq 1/\pi$. Beyond this value of F, increasing the order of mode coupling in Eq. (4.9) does not guarantee that the approximation improves. Accordingly, there is an optimal finite order of approximation for a given value of ε as usual in asymptotic series. In this sense, our results above seem to indicate that Eq. (4.9) is the optimal approximation for the mode $k=1$ in the asymptotic (nonconvergent) region (i.e., for moderately long times).

In the same spirit of Eq. (4.9), we can also derive a closed system of differential equations, which includes third-order couplings for the modes $k=1,3$ by replacing $\lambda(k)\delta_k$ with $\dot{\delta}_k$ for the modes $k=1,3$ in Eq. (3.23). The system reads

$$\dot{\beta}_1 = \frac{1}{2}\beta_1 - \frac{1}{4}\beta_1^2\dot{\beta}_1 - \beta_3^2\dot{\beta}_1 - \frac{1}{2}\beta_1\beta_3\dot{\beta}_3 + \frac{1}{2}\beta_1\beta_3\dot{\beta}_1, \tag{4.11}$$

$$\dot{\beta}_3 = \frac{3}{2}\beta_3 - \frac{3}{2}\beta_1\beta_3\dot{\beta}_1 - \frac{9}{4}\beta_3^2\dot{\beta}_3. \tag{4.12}$$

Numerical solution (referred to as ''Resummation, $k=1,3$'' in the figures) of these equations shows no qualitative differences with the case of the single mode $k=1$, as far as the flux and the amplitude of the first mode are concerned. The improvement in the amplitude of the third mode and consequently in the shape of the finger does not reach the high values of F that the first mode reaches ($F \simeq 0.8$), as we can see in Fig. 8. In a short range of F the mode $k=3$ is better than the case shown in the previous section, but deviates from the exact solution much earlier than the mode $k=1$ for the same reasons as in the previous section. Specifically the mode $k=3$ is extremely good until $F \simeq 0.25$, starts deviating by more than 10% at $F \simeq 0.33$, and is about 50% of the value at $F \simeq 0.40$.

We conclude that the weakly nonlinear formalism, apart from its nominal range of validity for very small amplitudes where it converges very fast to the exact dynamics, can describe regimes beyond those expected, *a priori*, with reasonable accuracy. In the case of the growth of a single finger, for instance, we have explicitly seen that only two modes together with an appropriate partial resummation, yield a remarkably good approximation in the full range of convergence of the expansion ($F<1/\pi$).

V. CONCLUSION AND PERSPECTIVES

A systematic scheme to derive the successive orders of mode couplings in a weakly nonlinear regime, adapted to the study of interfacial dynamics in Hele-Shaw flows has been developed. In this paper we have applied the method to the channel geometry driven by gravity and pressure. The method could also be applied to even more general (position-dependent) driving. The formulation in real space has enabled us to address the issue of convergence of the mode-coupling expansion. We have found that the exact condition for convergence in the channel geometry is $|h_x|<1$ at every point of the interface.

The explicit derivation of nonlinear couplings up to third order in the case of channel geometry has been done in order to obtain the leading nonlinear contributions in cases where the second-order contribution vanishes. These include the case of zero viscosity contrast and the time-dependent single-finger solution of width $\lambda=\frac{1}{2}$.

On the analytical side, the usefulness of the weakly nonlinear analysis in elucidating the role of the different parameters on the dynamics, in some examples, has been demonstrated. In the case of single-finger solutions growing in a channel, we have shown how an exact nontrivial property of the problem (the relationship between λ and viscosity contrast A for zero surface tension) can be extracted from an analysis order by order, without really knowing the exact solution.

On the numerical side, the predictions of the weakly nonlinear analysis, at different orders, against exact solutions have been checked. We have found that the convergence is quite fast for small amplitudes. Furthermore, in the case of a single finger growing in a channel we have explicitly seen that the analysis of low orders (up to three-mode couplings) yields a good description of the interface dynamics even close to the radius of convergence. With an appropriate resummation scheme, the prediction is relatively good even beyond this point.

Some of the most interesting applications of the systematic weakly nonlinear approach have not been developed here since they deserve a separate, in-depth analysis. The first is the application of the present scheme to the radial geometry with arbitrary injection and centrifugal driving, which includes the case of a rotating Hele-Shaw cell. The analysis in this case presents a number of specific features and it has been performed explicitly up to second-order couplings in [36]. A thorough discussion of this geometry, including the convergence analysis, will be presented in a forthcoming paper. Another possible interesting application is the study of the scaling properties of fluctuations in stable stratified Hele-Shaw flows with external noise [28]. Finally, a more direct application of our formalism, which also deserves a separate analysis, is the derivation of amplitude equations for the region near the instability threshold through a center manifold reduction. This would come under what is most commonly referred to as the ''weakly nonlinear'' approach in the literature of pattern formation. A detailed study of this point with a careful discussion of the nature of the bifurcation and its implications will be presented elsewhere.

ACKNOWLEDGMENTS

We acknowledge financial support from the Dirección General de Enseñanza Superior (Spain) under Projects No. BXX2000-0638-C02-02. E.A.L. also acknowledges a grant from the Comissionat per a Universitats i Recerca of the Generalitat de Catalunya. The work was also supported by the European Commission Project No. ERB FMRX-CT96-0085 (Training and Mobility of Researchers).

[1] D. Bensimon, L. Kadanoff, S. Liang, B. I. Shraiman, and C. Tang, Rev. Mod. Phys. **58**, 977 (1986).
[2] P. G. Saffman, J. Fluid Mech. **173**, 73 (1986).
[3] P. Pelcé, *Dynamics of Curved Fronts* (Academic Press, San Diego, 1988).
[4] J. S. Langer, in *Chance and Matter, 1986* Les Houches Lectures in the Theory of Pattern Formation, edited by J. Souletie, J. Vannimenus, and R. Stora (North-Holland, Amsterdam, 1987).
[5] D. Kessler, J. Koplik, and H. Levine, Adv. Phys. **37**, 255 (1988).
[6] M. C. Cross and P. C. Hohenberg, Rev. Mod. Phys. **65**, 851 (1993).
[7] P. G. Saffman and G. I. Taylor, Proc. R. Soc. London, Ser. A **245**, 312 (1958).
[8] P. Manneville, *Dissipative Structures* (Springer-Verlag, Berlin, 1990).
[9] L. Paterson, J. Fluid Mech. **113**, 513 (1981).
[10] J. D. Chen, J. Fluid Mech. **201**, 223 (1989).
[11] G. Tryggvason and H. Aref, J. Fluid Mech. **136**, 1 (1983).
[12] D. C. Hong and J. S. Langer, Phys. Rev. Lett. **56**, 2032 (1986).
[13] B. I. Shraiman, Phys. Rev. Lett. **56**, 2028 (1986).
[14] R. Combescot, T. Dombre, V. Hakim, Y. Pomeau, and A. Pumir, Phys. Rev. Lett. **56**, 2036 (1986).
[15] S. Tanveer, Philos. Trans. R. Soc. London, Ser. A **343**, 155 (1993).
[16] M. Siegel and S. Tanveer, Phys. Rev. Lett. **76**, 419 (1996).
[17] M. Siegel, S. Tanveer, and W. S. Dai, J. Fluid Mech. **323**, 201 (1996).
[18] J. Casademunt and F. X. Magdaleno, Phys. Rep. **337**, 1 (2000).
[19] G. Tryggvason and H. Aref, J. Fluid Mech. **154**, 287 (1985).
[20] J. V. Maher, Phys. Rev. Lett. **54**, 1498 (1985).
[21] M. W. Difranceso and J. V. Maher, Phys. Rev. A **39**, 4709 (1989).
[22] M. W. Difranceso and J. V. Maher, Phys. Rev. A **40**, 295 (1989).
[23] J. Casademunt and D. Jasnow, Phys. Rev. Lett. **67**, 3677 (1991).
[24] J. Casademunt and D. Jasnow, Physica D **79**, 387 (1994).
[25] P. Jacquar and P. Séguer, J. Mec. **1**, 367 (1962).

[26] R. Folch, E. Pauné, and J. Casademunt (unpublished).
[27] Ll. Carrillo, F. X. Magdaleno, J. Casademunt, and J. Ortín, Phys. Rev. E **54**, 6260 (1996).
[28] A controlled experiment of quenched noise in a Hele-Shaw cell with stably stratified flow has been recently proposed by J. Soriano, J. Ortín, and A. Hernández-Machado (unpublished).
[29] L. W. Schwartz, Phys. Fluids A **1**, 167 (1989).
[30] Ll. Carrillo, J. Soriano, and J. Ortín, Phys. Fluids **11**, 778 (1999).
[31] Ll. Carrillo, J. Soriano, and J. Ortín, Phys. Fluids **12**, 1685 (2000).
[32] V. M. Entov, P. I. Etingof, and D. Ya. Kleinbock, Eur. J. Appl. Math. **6**, 399 (1995).
[33] D. G. Crowdy, Q. Appl. Math. (to be published).
[34] F. X. Magdaleno, A. Rocco, and J. Casademunt, Phys. Rev. E **62**, R5887 (2000).
[35] E. Alvarez-Lacalle, J. Ortín, and J. Casademunt (unpublished).
[36] E. Alvarez-Lacalle, J. Casademunt, and J. Ortín, e-print nlin-ps/0011049.
[37] H. Guo, D. C. Hong, and D. A. Kurtze, Phys. Rev. Lett. **69**, 1520 (1992).
[38] H. Guo, D. C. Hong, and D. A. Kurtze, Phys. Rev. E **51**, 4469 (1995).
[39] J. A. Miranda and M. Widom, Int. J. Mod. Phys. B **12**, 931 (1998).
[40] J. A. Miranda and M. Widom, Physica D **120**, 315 (1998).
[41] R. E. Goldstein, A. I. Pesci, and M. J. Shelley, Phys. Fluids **10**, 2701 (1998).